catalysts

MDPI

Article

Efficient Waste to Energy Conversion Based on Co-CeO_2 Catalyzed Water-Gas Shift Reaction

Kyoung-Jin Kim [1], Yeol-Lim Lee [1], Hyun-Suk Na [1], Seon-Yong Ahn [1], Jae-Oh Shim [2,*], Byong-Hun Jeon [3,*] and Hyun-Seog Roh [1,*]

1 Department of Environmental Engineering, Yonsei University, 1 Yonseidae-gil, Wonju, Gangwon-do 26493, Korea; kyoungjinkim@yonsei.ac.kr (K.-J.K.); yllee@yonsei.ac.kr (Y.-L.L.); hsna@yonsei.ac.kr (H.-S.N.); syahn99@yonsei.ac.kr (S.-Y.A.)

2 Department of Chemical Engineering, Wonkwang University, 460, Iksan-daero, Iksan-si, Jeollabuk-do 54538, Korea

3 Department of Earth Resources and Environmental Engineering, Hanyang University, 222 Wangsimni-ro, Seongdong-gu, Seoul 04763, Korea

* Correspondence: joshim85@wku.ac.kr (J.-O.S.); bhjeon@hanyang.ac.kr (B.-H.J.); hsroh@yonsei.ac.kr (H.-S.R.)

Received: 13 March 2020; Accepted: 10 April 2020; Published: 12 April 2020

Abstract: Waste to energy technology is attracting attention to overcome the upcoming environmental and energy issues. One of the key-steps is the water-gas shift (WGS) reaction, which can convert the waste-derived synthesis gas (H_2 and CO) to pure hydrogen. Co–CeO_2 catalysts were synthesized by the different methods to derive the optimal synthetic method and to investigate the effect of the preparation method on the physicochemical characteristics of Co–CeO_2 catalysts in the high-temperature water-gas shift (HTS) reaction. The Co–CeO_2 catalyst synthesized by the sol-gel method featured a strong metal to support interaction and the largest number of oxygen vacancies compared to other catalysts, which affects the catalytic activity. As a result, the Co–CeO_2 catalyst synthesized by the sol-gel method exhibited the highest WGS activity among the prepared catalysts, even in severe conditions (high CO concentration: ~38% in dry basis and high gas hourly space velocity: 143,000 h^{-1}).

Keywords: waste-derived synthesis gas; high-temperature water-gas shift; Co–CeO_2 catalyst; preparation method; oxygen vacancy

1. Introduction

Economic development and population growth have increased the amount of globally generated waste, which is expected to rise from 2.0 billion tons per year in 2016 to 3.4 billion tons per year in 2050 [1,2]. Consequently, much attention has been directed at the development of waste to energy technologies such as waste gasification to reduce the extent of landfill depletion, environmental pollution, and waste treatment costs [3–5]. Notably, waste gasification can reduce waste mass (by ~80%) and volume (by ~90%), save landfill space, and decrease the emission of pollutants such as NO_x and SO_x [3].

Waste gasification typically affords synthesis gas (H_2 and CO), which can be used to generate value-added products such as synthetic crude oil, methanol, and dimethyl ether, and can also be employed as a substitute of reformed natural gas for pure H_2 production through the water-gas shift (WGS) reaction ($CO + H_2O \rightarrow CO_2 + H_2$) [4,6–9].

The growing importance of fuel-cell-based vehicles and related devices has increased the demand for H_2, used as a fuel in fuel cells [10–13]. However, more than 96% of H_2 is generated from natural gas- and petroleum-derived sources (i.e., from fossil fuels), which highlights the need for practical

alternative sources such as waste. In particular, combustible waste with minimum calorific value (4000–5000 kcal kg^{-1}) can be gasified to afford synthesis gas containing CO (~38%) and H_2 (~28%), along with relatively small amounts of CH_4, CO_2, N_2, and other impurities [14].

The WGS reaction is exothermic and is thus favored by low temperatures. Therefore, according to thermodynamic limitations and kinetic aspects, the WGS reaction can be conducted in two distinct temperature ranges, namely at 350–550 °C (high-temperature shift, HTS) over Fe_2O_3–Cr_2O_3 and at 190–250 °C (low-temperature shift, LTS) over CuO–ZnO–Al_2O_3 [15,16]. Due to the high outlet temperature of the waste gasification process (>500 °C), HTS is better suited for H_2 production through waste gasification than LTS [17,18]. However, commercial Fe_2O_3–Cr_2O_3 catalysts are not suitable for the HTS reaction of waste-derived synthesis gas, as the high CO levels of this feedstock (~38% CO, cf. ~9% CO of natural gas-derived synthesis gas) may lead to rapid catalyst deactivation [19]. Hence, customized catalysts for waste-derived synthesis gas processing are highly sought after. Furthermore, upon operation, Cr^{3+} present in fresh Fe_2O_3–Cr_2O_3 catalysts is oxidized to Cr^{6+}, which may leach out from spent catalysts to cause environmental and health problems [8,20]. For this reason, the replacement of Cr for other metals in commercial HTS catalysts is also required [21].

Previously, we have developed a Co-based catalyst for H_2 production from waste-derived synthesis gas via the HTS reaction, showing that this catalyst exhibits high activity in a wide temperature range and at high gas hourly space velocity (GHSV) to demonstrate the feasibility of using Cr-free catalysts [8,22–25]. Compared to the unsupported Co_3O_4 catalyst, CeO_2-supported Co catalysts featured enhanced stability and redox activity [22,23]. This behavior was attributed to the strong interaction between Co and the CeO_2 support, which prevented the sintering of the Co^0 active phase [17,25]. In addition, the large amount of oxygen defects in the Co–CeO_2 catalyst resulted in high CO conversion [8,24].

In general, CeO_2 is known as an active substance that drives water dissociation in the WGS reaction. Additionally, it shows unique redox properties and promotes the formation of oxygen vacancies. The formation of oxygen vacancies can be interpreted as the generation of mobile oxygen on the CeO_2 surface, improving the catalytic activity in the WGS reaction [22]. In addition, CeO_2 features the improved oxidative strength and photoelectronic activity due to unique solid-state reactivity of Ce [26]. Arena et al. developed the nanocomposite $MnCeO_x$ catalyst, and proved that Ce promotes the dispersion of the active metals and the exposure of the active sites at the surface of the catalyst [27–31]. As has been widely reported, the use of CeO_2, which has unique properties in a variety of catalytic chemical reactions including the WGS reaction, is prevalent. Accordingly, changes in redox properties and oxygen storage capacity (OSC) of catalysts by applying the Ce have been investigated in various literatures. The Co_3O_4 catalyst for total oxidation of propene enhanced the mobility of lattice oxygen by applying the CeO_2 support, and the mobile oxygen reacts with the propene, showing high catalytic activity [32]. Au/CeO_2–ZnO/Al_2O_3 catalyst showed excellent performance in the WGS reaction because of the enhanced oxygen storage capacity and reducibility [33]. The Au/Co_x/CeO_2–Al_2O_3 catalyst showed outstanding activity in the CO oxidation reaction due to the superior redox properties and oxygen storage/release properties of CeO_2 [34].

Many attempts have been made to enhance catalyst performance through the optimization of preparation methods [35–42]. Wang et al. prepared MgAl catalysts for dehydroxylation by a sol-gel technique, showing that the generation of oxygen defects is influenced by the choice of synthesis method [35]. Kakihana et al. observed that the sol-gel method affords catalysts with higher homogeneity/purity in the form of powders with submicron particle size [36]. In addition, the sol-gel method has also been reported to be highly economical because of the reduced catalyst preparation time and cost [37]. Avgouropoulos et al. ascribed the improved catalytic performance of hydrothermally prepared CuO–CeO_2 catalysts for the selective CO oxidation to the high dispersion of CuO and its strong interaction with the CeO_2 support [38]. The enhanced CO oxidation activity of the co-precipitation-prepared catalyst was attributed to the increased surface area of CeO_2 and the enhanced redox properties due to Ce–Fe–O solid solution formation [39]. Megarajan et al. claimed

that the high diesel soot oxidation activity of a Co_3O_4–CeO_2 catalyst prepared by incipient wetness impregnation was due to the high dispersion of Co_3O_4 nanoparticles on the CeO_2 support [40]. Although the preparation method strongly affects catalyst performance, no related research has been conducted in the case of Co-based catalysts for the HTS reaction using waste-derived synthesis gas.

Herein, we probe the effects of the preparation method (sol-gel, co-precipitation, incipient wetness impregnation, and hydrothermal) on the physicochemical characteristics of Co–CeO_2 catalysts and establish an optimal preparation method by comparing their activities for the HTS reaction using waste-derived synthesis gas. Moreover, correlations between catalyst physicochemical characteristics and activity are discussed.

2. Results and Discussion

2.1. Catalyst Characterization

Table 1 lists the physicochemical properties of Co–CeO_2 catalysts synthesized by various methods, revealing that the Brunauer-Emmett-Teller (BET) area decreased after the reaction (30–82 $m^2\ g^{-1}$ for fresh catalysts vs. 24–73 $m^2\ g^{-1}$ for used catalysts).

Table 1. Characteristics of Co–CeO_2 catalysts prepared by different synthetic methods.

Catalysts	Surface Area (m^2/g) [a]		Dispersion (%) [b]		O_2^{2-}/O^{2-} [c]	Ce^{3+} (%) [c]	OSC (10^{-5} gmol/g_{cat}) [d]
	Fresh	Used	Fresh	Used			
Co–CeO_2 (SG)	30	24	1.61	0.42 (74% ↓)	0.50	44.6	3.9
Co–CeO_2 (IWI)	82	65	1.91	0.17 (91% ↓)	0.43	43.8	2.8
Co–CeO_2 (CP)	82	73	1.09	0.15 (86% ↓)	0.37	40.7	2.6
Co–CeO_2 (HT)	69	48	2.14	0.68 (68% ↓)	0.29	36.9	2.5

[a] Estimated from N_2 adsorption at −196 °C. [b] Calculated from CO-chemisorption. [c] Estimated from X-ray photoelectron spectroscopy (XPS). [d] Calculated from H_2-O_2 pulse reaction.

As a result of measuring the cobalt dispersion through CO-chemisorption (Table 1), the Co–CeO_2 (HT) catalyst featured the highest Co dispersion in both fresh and used forms. For all catalysts, dispersion decreased after the reaction, which was ascribed to active metal sintering [43]. In particular, the Co–CeO_2 (IWI) catalyst showed the highest decrease rate (91% ↓) among the prepared catalysts. The Co–CeO_2 (SG) catalyst and Co–CeO_2 (CP) catalyst showed a relatively higher decrease rate (SG: 74% ↓, CP: 86% ↓) compared to the Co–CeO_2 (HT) catalyst (68% ↓). Thus, even for catalysts with identical Co loadings, Co dispersion depended on the synthetic method, being the lowest for catalysts prepared using sol-gel or co-precipitation methods, which was ascribed to the partial coverage of metal on the surface [44].

Figure 1 presents the X-ray diffraction (XRD) patterns of different Co–CeO_2 catalysts, showing that all major diffraction peaks were consistent with the fluorite-type structure of CeO_2 [25]. Peaks at 2 theta = 31.2, 36.9, 45.0, and 65.2° observed for all fresh samples (Figure 1a) were attributed to the (220), (311), (400), and (440) reflections of Co_3O_4, respectively [45]. The patterns of all used catalysts featured a small diffraction peak of Co^0 at 2 theta = 44.2° (Figure 1b), which confirmed the formation of Co^0 from Co_3O_4 due to the pre-reaction reduction.

Catalyst structure and oxygen vacancy concentration were probed by Raman spectroscopy. As shown in Figure 2a, all catalysts showed peaks that correspond to Co_3O_4 and CeO_2 [46]. In here, the peak at ~457 cm^{-1}, which is attributed from the F_{2g} vibration mode of the fluorite structure of CeO_2, was deconvoluted and magnified in Figure 2b to focus on the feature of this peak in each sample. Interestingly, in the case of the Co–CeO_2 (SG) catalyst, this peak was clearly shifted to lower wave numbers, which was indicative of CeO_2 structural distortion that generated lattice strain and defects in the CeO_2 lattice, and thus promoted the formation of oxygen vacancies [47,48]. This indicates that the largest amount of oxygen vacancy was formed in the Co–CeO_2 (SG) catalyst. In our previous research, we confirmed that oxygen vacancy concentration is related to catalytic performance in the WGS reaction [18]. The WGS reaction at the high temperature range occurs through the redox mechanism.

In the high-temperature WGS reaction, CO molecules are adsorbed at catalyst active sites and oxidized to CO_2 by the lattice oxygen in CeO_2, which results in the formation of oxygen vacancies. Subsequently, steam (H_2O) dissociation on the catalyst surface regenerates lattice oxygen and affords H_2. As high levels of oxygen vacancies facilitate the oxidation of CO to CO_2, the Co–CeO_2 (SG) catalyst is expected to show the highest HTS activity [14]. Therefore, it is expected that the Co–CeO_2 (SG) catalyst will show higher activity than other catalysts for the HTS reaction due to the large number of oxygen vacancies. Oxygen vacancy formation was further confirmed by X-ray photoelectron spectroscopy (XPS) and oxygen storage capacity (OSC) measurements.

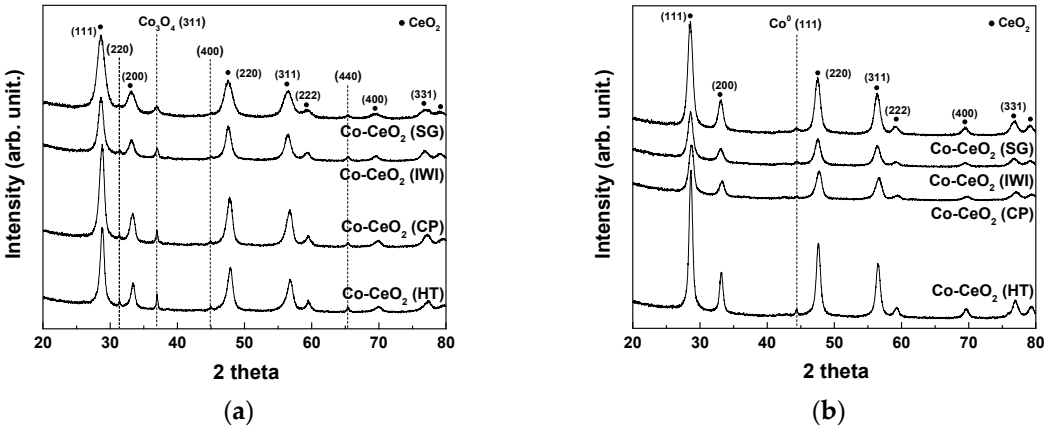

Figure 1. X-ray diffraction (XRD) patterns of Co–CeO_2 catalysts prepared by different synthetic methods: (**a**) Fresh, (**b**) Used.

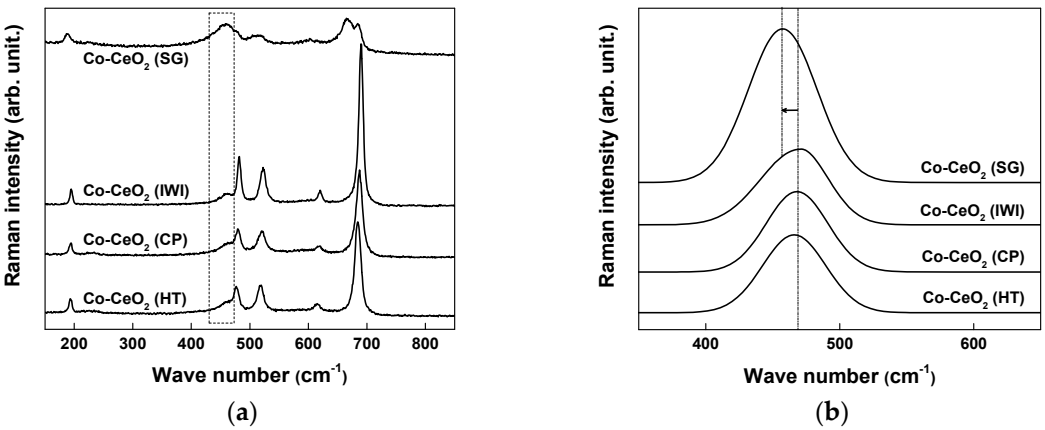

Figure 2. Raman spectroscopy results of Co–CeO_2 catalysts prepared by different synthetic methods. (**a**) Wide range of 150~850 cm^{-1}, (**b**) Magnified results to focus the peak at ~457 cm^{-1}.

The relative content of defect oxygen and the valence states of O, Ce, and Co in Co–CeO_2 catalysts were determined by XPS. The O 1s spectra of all samples (Figure 3a) were deconvoluted into the peaks of lattice oxygen (528.9 eV), oxygen close to oxygen vacancy sites (530.3 eV), and surface-adsorbed oxygen species from hydroxyl groups or water (532.2 eV) [17]. The relative contents of these species were calculated from the areas of the corresponding peaks. As defect oxygen is generated from oxygen vacancies, the defect oxygen to lattice oxygen (O_2^{2-}/O^{2-}) ratio is related to the concentration of oxygen vacancies. The obtained results are listed in Table 1 and demonstrate that the above ratio was the highest for the Co–CeO_2 (SG) catalyst, which was in good agreement with the results of the Raman spectroscopic characterization. The Ce 3d spectra of the Co–CeO_2 catalysts (Figure 3b) were deconvoluted into 10 peaks corresponding to different Ce oxidation states (Ce^{4+} and Ce^{3+}). According

to the references, peaks marked as v_0, v, v', v'', and v''' and u_0, u, u', u'', and u''' were attributed to Ce $3d_{5/2}$ and Ce $3d_{3/2}$, respectively. Peaks marked as v, v'', v''', u, u'', and u''' were assigned to Ce^{4+}, while those denoted as v_0, v', u_0, and u' were attributed to Ce^{3+} [25,49]. The generation of oxygen vacancies resulted in the reduction of Ce^{4+} to Ce^{3+} on the catalyst surface, providing the active sites for water dissociation. The relative content of Ce^{3+} in Ce 3d spectra was calculated by considering the presence of Ce^{3+} ions directly involved in the dissociation of water. As a result, the Co–CeO_2 (SG) catalyst showed the highest Ce^{3+} concentration, in agreement with the results of the Raman spectroscopic analysis and the defect oxygen to lattice oxygen ratio (O_2^{2-}/O^{2-}) [8]. The Co $2p_{3/2}$ spectra of the Co–CeO_2 catalyst in the binding energy ranging from 776 to 786 eV are shown in Figure 3c. According to the literature, the spectra can be attributed to the Co^{2+} and Co^{3+} species, which were located at 781.0 ± 0.4 and 779.4 ± 0.4 eV, respectively [50–53]. These peaks revealed the coexistence of Co_3O_4 and CoO species on the surface of the catalysts. Based on the above XPS results, we expected the Co–CeO_2 (SG) catalyst to show the highest activity among the prepared catalysts due to its larger number of oxygen vacancies.

OSC was calculated by performing pulse reactions with H_2 as the reductant and O_2 as the oxidant. O_2 oxidized the catalyst oxygen vacancies, while Ce^{4+} was reduced to Ce^{3+} by H_2. The amount of consumed O_2 coincided with the OSC (Table 1), increasing in the order of Co–CeO_2 (HT) < Co–CeO_2 (CP) < Co–CeO_2 (IWI) < Co–CeO_2 (SG). Thus, the Co–CeO_2 (SG) catalyst featured the highest OSC (and, hence, the largest oxygen vacancy concentration), in accordance with the Raman spectroscopy and XPS results.

The reduction properties of the Co–CeO_2 catalysts were probed by H_2-temperature programmed reduction (H_2-TPR) measurements (Figure 4), with two main reduction peaks observed for all samples. The first peak at 211–327 °C was attributed to the reduction of Co_3O_4 to CoO, while the second one at 262–414 °C represented the reduction of CoO to Co^0. The temperature of the first peak increased in the order of Co–CeO_2 (HT) < Co–CeO_2 (SG) < Co–CeO_2 (CP) < Co–CeO_2 (IWI), while that of the second peak increased in the order of Co–CeO_2 (HT) < Co–CeO_2 (CP) < Co–CeO_2 (IWI) < Co–CeO_2 (SG) (i.e., the reduction of CoO to the Co^0 in Co–CeO_2 (SG) catalyst occurred at the highest temperature). This means that the active species in HTS, Co^0 (metallic cobalt), is formed at higher temperature than other catalysts in the case of the Co–CeO_2 (SG) catalyst. Thus, we concluded that the use of the sol-gel method for Co–CeO_2 catalyst preparation may improve the interaction between Co^0 and the CeO_2 support. The strong metal–support interaction (SMSI) is an important factor that affects both catalytic activity and stability (e.g., catalysts with SMSI show high performance) [54–56]. Interestingly, the CoO reduction temperature of the prepared catalysts (described as the SMSI) followed the same trend as the defect oxygen to lattice oxygen ratio, showing that the SMSI induces the generation of oxygen vacancies. Similar findings were reported by Fichtl et al., which describe that the formation of oxygen vacancy is related to the interaction between active metal and support [57,58]. As a result, it is in-line that the Co–CeO_2 (SG) showed the SMSI estimated by H_2-TPR result, with the aforementioned description in the XPS and Raman results, which proves that Co–CeO_2 (SG) showed a large number of oxygen vacancies.

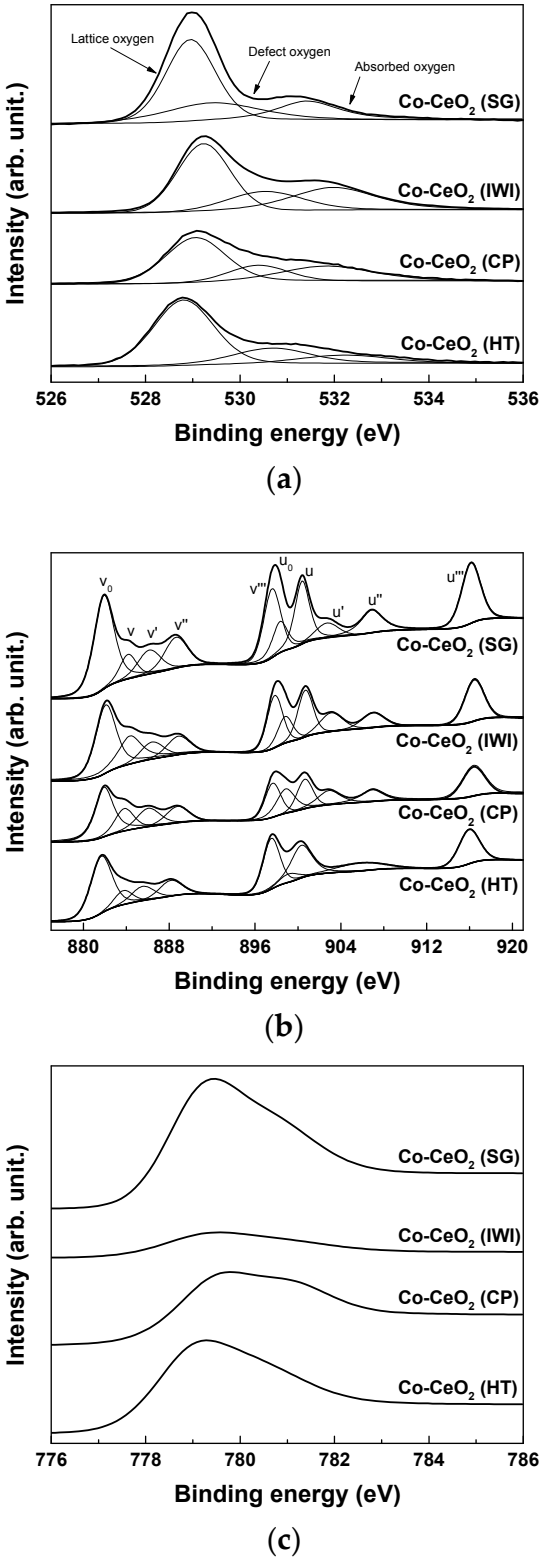

Figure 3. X-ray photoelectron spectroscopy (XPS) patterns of Co–CeO_2 catalysts prepared by different synthetic methods: (**a**) O 1s, (**b**) Ce 3d, (**c**) Co 2p.

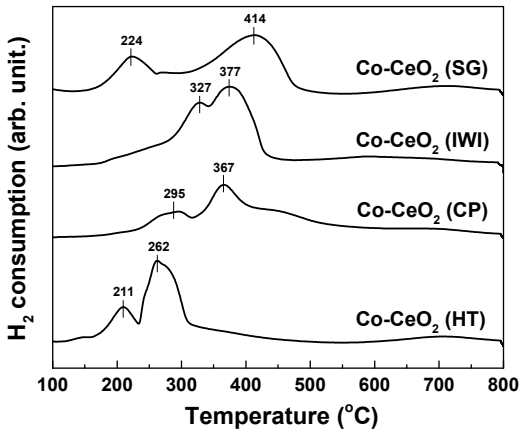

Figure 4. H_2-temperature programmed reduction (H_2-TPR) profiles of Co–CeO_2 catalysts prepared by different synthetic methods.

2.2. Reaction Results

The catalytic activity test was conducted in the temperature range of 400–550 °C to determine the most effective method of Co–CeO_2 catalyst synthesis (Figure 5). Among the prepared catalysts, the Co–CeO_2 (SG) catalyst showed the highest CO conversion (~90%) across the entire tested temperature range, whereas the Co–CeO_2 (HT) catalyst showed the lowest CO conversion (~39%). The activity of the Co–CeO_2 (IWI) catalyst at 400 °C was close to that of the Co–CeO_2 (SG) catalyst, but decreased at higher temperatures. To sum up, catalyst performance was strongly related to the reduction properties of CoO, which can be described in terms of the SMSI and oxygen vacancy concentration. Oxygen vacancies are known to actively participate in the WGS reaction and promote the diffusion of lattice oxygen [17,59]. Hence, the SMSI effect-related generation of oxygen vacancies resulted in increased catalytic activity. In addition, the catalyst oxygen storage capacity depended on the preparation method and also affected catalytic activity, whereas physicochemical properties such as BET surface area and catalyst dispersion were believed to have less influence.

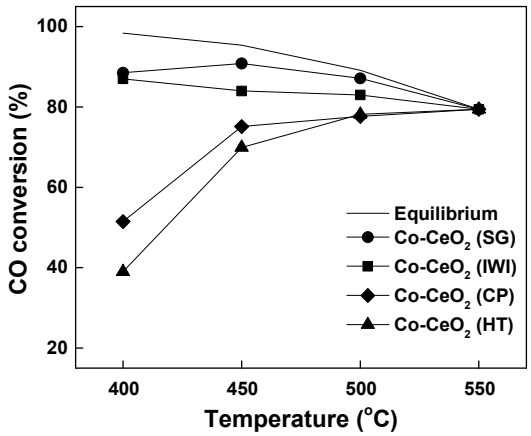

Figure 5. CO conversion with reaction temperature over Co–CeO_2 catalysts prepared by different synthetic methods ($H_2O/(CH_4 + CO + CO_2) = 2.0$; GHSV = 143,000 h^{-1}).

To identify the methanation reaction ($CO + 3H_2 \rightarrow CH_4 + H_2O$), which is a side reaction of the WGS reaction, the selectivities to CO_2 and CH_4 were calculated and shown in Figure 6. Except for Co–CeO_2 (HT) catalyst (96% CO_2 selectivity), the catalysts showed a CO_2 selectivity of 100%, which indicated that methanation did not occur. Thus, the Co–CeO_2 (SG) catalyst showed the highest catalytic activity without any side reactions, and its potential was further probed by an additional stability test performed at 450 °C and a GHSV of 143,000 h^{-1} for 20 h.

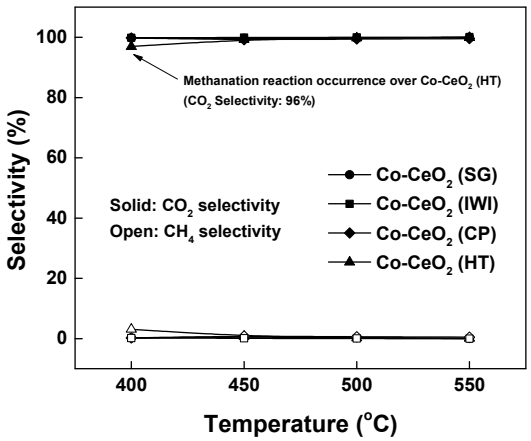

Figure 6. Selectivity to CO_2 and CH_4 with reaction temperature over Co–CeO_2 catalysts prepared by different synthetic methods ($H_2O/(CH_4 + CO + CO_2)$ = 2.0; gas hourly space velocity (GHSV) = 143,000 h^{-1}).

In the case of the primary stability test of Co–CeO_2 (SG) catalyst, the test was performed under the reaction conditions of 450 °C and GHSV = 143,000 h^{-1} to examine the stability of Co–CeO_2 (SG) catalyst in the HTS reaction. Figure 7 indicates that the Co–CeO_2 (SG) catalyst showed excellent stability, almost reaching the equilibrium CO conversion and maintaining activity up to 20 h, even in the very high GHSV of 143,000 h^{-1}. However, we tried to check the potentially higher activity and stability that may be limited by the thermodynamic equilibrium. Due to this reason, we repeated the stability test in the condition where the catalyst may show lower activity than the thermodynamic equilibrium (T = 400 °C, GHSV = 203,000 h^{-1}). Although the Co–CeO_2 (SG) catalyst showed the most outstanding activity among the prepared catalysts, it was found that the stability of the catalyst gradually decreased within 20 h in the newly established reaction condition. From this result, further study on the development of catalysts for HTS reaction using waste-derived synthesis gas with improved stability seems to be necessary for its application in the industrial field.

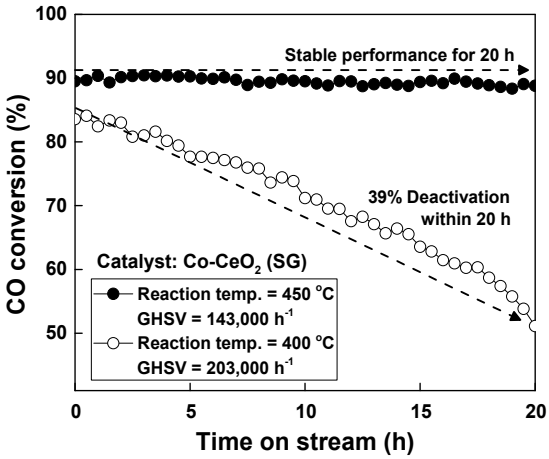

Figure 7. CO conversion with time on stream over Co–CeO_2 (SG) catalysts ($H_2O/(CH_4 + CO + CO_2)$ = 2.0; T = 400 and 450 °C; GHSV = 203,000 and 143,000 h^{-1}).

In order to confirm the catalytic performance of the Co–CeO_2 (SG) catalyst, the performance was compared with the pre-developed Co and Ce based catalysts for HTS reaction through the literature survey in Table 2 [60–64]. The Co–CeO_2 (SG) catalyst developed in this study showed superior catalytic performance to reach the equilibrium CO conversion, even at a relatively high CO concentration

(17.02 vol.%) and GHSV (143,000 h^{-1}). As a result, it was confirmed that the synthesis of a Co-based catalyst for HTS reaction using waste gasification synthesis gas was successfully achieved.

Table 2. Comparative results of Co and Ce based catalysts for the high-temperature shift reaction.

Catalysts (Preparation Method)	Reaction Condition			Conversion		Reference
	GHSV or Flow Rate	Feed Gas Ratio	Press (bar)	Reaction Temp. (°C)	CO Conv. [Equil. CO Conv.] (%)	
15%Co–CeO_2 (Sol-gel method)	143,000 h^{-1}	17.02% CO, 9.55% CO_2, 1.03% CH_4, 13.14% H_2, 55.20% H_2O, 4.06 %N_2	1	450	**~90** [~95]	This work
10%Co/CeO_2-spindles (Wet impregnation method)	6000 h^{-1}	7.5% CO, 3% CO_2, 27.5% H_2, 50% H_2O, 12% N_2	1	300	**~91** [~95]	[60]
1%Au–10%Co_3O_4/CeO_2 (Deposition precipitation method)	12,000 h^{-1}	4% CO, 3% CO_2, 37.9 H_2, 9.4% H_2O, 45.7% He	1	350	**~30** [~60]	[61]
1%Co/Ce5%SmO (Impregnation method	100 mL min^{-1}	5% CO, 10% H_2O, 85% N_2	1	450	**~86** [~88]	[62]
Pd/$Co_{0.1}Ce_{0.6}Zr_{0.3}O_x$ (Impregnation method)	50,000 h^{-1}	2% CO, 5% H_2O, 93% N_2	1	400	**~95**	[63]
$Cu_{0.1}Co_{0.1}Ce_{0.8}O_2$ (nano-replication method)	64 mL min^{-1}	3% CO balanced with He and H_2O	1	350	**~99**	[64]

In the present study, the Co–CeO_2 catalyst activity result was influenced by the synthetic method. The high performance of the Co–CeO_2 (SG) catalyst can be explained as follows. First, oxygen vacancy concentration affects the HTS reaction. Raman spectroscopy, XPS, and H_2–O_2 pulse reaction results showed that the Co–CeO_2 (SG) catalyst had the highest concentration of oxygen vacancies among the prepared catalysts. As the WGS reaction primarily proceeds through a redox mechanism, it is strongly influenced by the concentration of oxygen vacancies. Liotta et al. developed the Co_3O_4–CeO_2 catalysts for the total oxidation of propene. The prepared catalysts showed increased surface oxygen vacancies through the application of a CeO_2 support and optimization of Co loading [32]. Reina et al. tested the gold catalysts supported on CeO_2–Al_2O_3 for CO oxidation. As a result of applying the transition metal oxides (Co_3O_4 or V_2O_5) to the CeO_2–Al_2O_3 support, the transportation of oxygen to the active sites of Co_3O_4-doped catalyst was improved due to CeO_2–CoO_x interaction [34]. In line with the reported studies, we have confirmed that the catalytic activity of Co–CeO_2 catalysts were improved through the enhancement of OSC. In this study, the OSC of the catalyst was critically affected by the catalyst preparation method. Second, the SMSI effect is important for the generation of oxygen vacancy, which is directly related to the catalytic activity. According to the TPR results, the CoO reduction temperature was highest for the Co–CeO_2 (SG) catalyst, which was ascribed to the SMSI of this catalyst. Similar findings were reported dealing with the relation between the redox properties of the catalyst and catalytic activity. Reina et al. studied Au/CeO_2/Al_2O_3 catalysts doped with ZnO for the WGS reaction and reported that the catalysts exhibited improved CeO_2 redox properties with the presence of ZnO [33]. Additionally, Reina et al. investigated Au/MO_x/CeO_2–Al_2O_3 catalysts and found that the interaction between gold and Co_3O_4 increased the reduction degree in the Co doped Au/CeO_2–Al_2O_3 systems [34]. As a result, the Co–CeO_2 (SG) catalyst showed the most outstanding catalytic activity in the HTS reaction due to the large number of oxygen vacancies induced by the strong interaction between cobalt and CeO_2 support, despite the extremely high GHSV and CO concentration.

3. Materials and Methods

3.1. Preparation of Catalysts

Co–CeO_2 (85 wt% CeO_2 support, 15 wt% Co) was prepared by sol-gel, co-precipitation, incipient wetness impregnation, and hydrothermal methods (Co–CeO_2 (SG), Co–CeO_2 (CP), Co–CeO_2 (IWI), and Co–CeO_2 (HT), respectively) using stoichiometric quantities of $Co(NO_3)_2{\cdot}6H_2O$ (Sigma-Aldrich, St. Louis, MO, USA) and $Ce(NO_3)_3{\cdot}6H_2O$ (Sigma-Aldrich, St. Louis, MO, USA). To obtain Co–CeO_2 (SG) catalyst, stoichiometric quantities of cobalt, cerium precursors, and citric acid (Sigma-Aldrich, St. Louis, MO, USA) were dissolved in deionized water (20 mL), and the solution was stirred at 80 °C

for 24 h. As the water evaporated, citric acid acted as a chelating agent to result in gel formation. After gelation, the product was dried at 100 °C for 4 h to afford a fluffy mass that was then calcined at 500 °C for 6 h. The Co–CeO_2 (CP) catalyst was prepared by treating a solution of $Co(NO_3)_2{\cdot}6H_2O$ and $Ce(NO_3)_3{\cdot}6H_2O$ with aqueous (15 wt%) KOH (Duksan, Ansan, Korea) to reach pH 10.5 at 80 °C. The precipitate was stirred for 72 h, washed with deionized water for five times, dried overnight at 100 °C, and calcined at 500 °C for 6 h. In the case of the Co–CeO_2 (IWI) catalyst, a solution of $Co(NO_3)_2{\cdot}6H_2O$ in deionized water (0.5 mL) was used to impregnate CeO_2 prepared by precipitation, as described above. The impregnation process was carried out by dropping one or two drops until the solution (0.5 mL) was completely consumed. The solid products were dried at 100 °C for 12 h in air and then calcined at 500 °C for 6 h in a furnace. To prepare the Co–CeO_2 (HT) catalyst, aqueous (15 wt%) NaOH (Duksan, Ansan, Korea) was injected into a solution of $Co(NO_3)_2{\cdot}6H_2O$ and $Ce(NO_3)_3{\cdot}6H_2O$ to reach pH 10 at 80 °C, and the mixture was stirred for 30 min for the precipitate to form. The suspension was held at 180 °C for 24 h in a hydrothermal reactor, washed with deionized water, dried overnight at 100 °C, and then calcined at 500 °C for 6 h.

3.2. Catalyst Characterization

Brunauer–Emmett–Teller (BET) surface areas were determined from N_2 adsorption/desorption isotherms recorded at 77 K using a ASAP 2010 device (Micromeritics, Norcross, GA, USA). Co dispersion was probed by CO-chemisorption at 50 °C (Autochem 2920, Micromeritics, Norcross, GA, USA) using 10% CO/He. X-ray diffraction (XRD) patterns were recorded for 2 theta = 20–80° using a Ultima IV diffractometer (Cu Kα radiation, 40 kV, 40 mA, Rigaku, Tokyo, Japan). Raman spectra (LabRam Aramis spectrometer, Horiba Jobin Yvon, Longjumeau, France) were recorded using the 532 nm excitation line of a Nd-YAG laser. X-ray photoelectron spectroscopy (XPS) measurements were performed on a K-Alpha spectrometer (Thermo-Scientific, Waltham, MA, USA) using monochromated Al Kα radiation. All spectra were adjusted using the reference C 1s binding energy of 284.6 eV. H_2-O_2 pulse reactions were carried out to calculate OSC. Specifically, catalysts were pretreated by heating for 2 h in He at 400 °C and exposed to an H_2 pulse (10% H_2/Ar) at the same temperature to consume mobile oxygen. The reduced catalysts were exposed to an O_2 pulse (10% O_2/Ar) to oxidize mobile oxygen, and OSC was calculated from the amount of consumed O_2. H_2-temperature programmed reduction (H_2–TPR) was performed in 10% H_2/Ar from 100 to 800 °C at a heating rate of 10 °C min^{-1} using a Micromeritics Autochem 2920 instrument. Detector sensitivity was calibrated by reduction of a known amount of NiO.

3.3. Catalyst Performance Test

Catalytic performance was tested at 400–550 °C in a fixed-bed microtubular quartz reactor at atmospheric pressure. Catalyst powder (0.03 g) was placed on quartz wool (catalyst bed) in a quartz reactor with an inner diameter of 4 mm, a thermocouple for measuring the reaction temperature was inserted into the catalyst bed, and the reactor was heated in a furnace. Before measurement, the catalyst was reduction-activated by heating for 2 h in 5% H_2/N_2 from room temperature to 400 °C, and the temperature was further held for 1 h, and then increased from 400 to 550 °C in 50 °C increments. The reactant gas comprised CO (17.02 vol%), CO_2 (9.55 vol%), CH_4 (1.03 vol%), H_2 (13.14 vol%), H_2O (55.20 vol%), and N_2 (4.06 vol%), which is typical of synthesis gas produced through waste gasification. Water was injected into the reactor using a syringe pump and vaporized at 180 °C upstream of the reactor. After the reaction, reactant and product gases were analyzed online by an Agilent 3000-micro gas chromatograph. The reaction temperature and inlet gas flow rate were maintained for 40 min during each temperature step in consideration of the time required for the reaction gas from the catalyst bed to reach the micro gas chromatograph. The outlet gas was chilled to 2.2 °C and passed through a trap to remove residual water before analysis by the micro gas chromatograph. The CO conversion of product gas for each temperature was determined as the five measurements performed in 3 min intervals. The feed $H_2O/(CH_4 + CO + CO_2)$ ratio was set to 2.0 to avoid coke formation. The GHSV

equaled 143,000 h^{-1}. The calculation of equilibrium conversion of CO was carried out using HSC 6.0 software (Version 6.0, Outotec, Espoo, Finland, 2006). The Gibbs free energy minimization method was applied, and the parameters related to the reaction including temperature, pressure, and reactant composition were altered. CO conversion and CO_2 and CH_4 selectivities were calculated as follows.

$$\text{CO conversion (\%)} = ([CO]_{in} - [CO]_{out})/[CO]_{in} \times 100 \quad (1)$$

$$CO_2 \text{ selectivity (\%)} = ([CO_2]_{out} - [CO_2]_{in})/(([CH_4]_{out} - [CH_4]_{in}) + ([CO_2]_{out} - [CO_2]_{in})) \times 100 \quad (2)$$

$$CH_4 \text{ selectivity (\%)} = ([CH_4]_{out} - [CH_4]_{in})/(([CH_4]_{out} - [CH_4]_{in}) + ([CO_2]_{out} - [CO_2]_{in})) \times 100 \quad (3)$$

4. Conclusions

Co–CeO_2 catalysts prepared by various synthetic methods were applied for the HTS reaction of waste-derived synthesis gas. The Co–CeO_2 (SG) catalyst showed the best performance, even under extremely harsh conditions (GHSV = 143,000 h^{-1}, CO conc. = 38.2% dry basis), when compared to the industrial HTS reaction condition (GHSV = 3000 h^{-1}, CO conc. = 10%). The outstanding performance of the developed catalyst was ascribed to the high concentration of oxygen vacancies, which is also related to the strong metal-support interaction. Raman spectroscopy, XPS, and H_2-O_2 pulse reaction data confirmed that the Co–CeO_2 (SG) catalyst had the high concentration of oxygen vacancies. Due to the formation of a larger number of oxygen vacancies induced by the strong interaction between the Co and CeO_2 support, the Co–CeO_2 (SG) catalyst showed the highest catalytic activity among the prepared catalysts. However, the stability test result conducted at 400 °C and accelerated GHSV (203,000 h^{-1}) showed that the developed catalyst gradually deactivated within 20 h. Based on the stability test results, a subsequent study will be conducted to design a catalyst capable of maintaining high stability and elucidate the mechanism of the catalyst deactivation.

Author Contributions: Conceptualization, K.-J.K. and Y.-L.L.; Data curation, K.-J.K., Y.-L.L., H.-S.N., and J.-O.S.; Formal analysis, K.-J.K. and Y.-L.L.; Funding acquisition, H.-S.R.; Investigation, K.-J.K.; Methodology, Y.-L.L. and H.-S.N.; Project administration, J.-O.S. and H.-S.R.; Resources, K.-J.K., Y.-L.L., and S.-Y.A.; Supervision, J.-O.S., B.-H.J., and H.-S.R.; Validation, K.-J.K.; Visualization, K.-J.K.; Writing-original draft, K.-J.K.; Writing-review & editing, K.-J.K., Y.-L.L., H.-S.N., S.-Y.A., and J.-O.S. All authors have read and agreed to the published version of the manuscript.

Funding: This work was supported by the National Research Foundation of Korea (NRF) grant funded by the Korean government (MSIT) (No. 2020R1A2B5B01002346).

Conflicts of Interest: The authors declare no conflicts of interest.

References

1. Kaza, S.; Yao, L.; Bhada-Tata, P.; Woreden, F.V. *What a Waste 2.0: A Global Snapshot of Solid Waste Management to 2050*, 1st ed.; World Bank: Washington, DC, USA, 2018; pp. 1–292.
2. Wilson, D.C.; Rodic, L.; Modak, P.; Soos, R.; Carpintero, A.; Velis, K.; Iyer, M.; Simonett, O. *Global Waste Management Outlook*; United Nations Environment Programme: Nairobi, Kenya, 2015; pp. 1–332.
3. Arena, U. Process and technological aspects of municipal solid waste gasification. A review. *Waste Manag.* **2012**, *32*, 625–639. [CrossRef] [PubMed]
4. Pereira, E.G.; Silva, J.N.; Oliveira, J.L.; Machado, C.S. Sustainable energy: A review of gasification technologies. *Renew. Sust. Energ. Rev.* **2012**, *16*, 4753–4762. [CrossRef]
5. Jang, W.-J.; Shim, J.-O.; Jeon, K.-W.; Na, H.-S.; Kim, H.-M.; Lee, Y.-L.; Roh, H.-S.; Jeong, D.-W. Design and scale-up of a Cr-free Fe-Al-Cu catalyst for hydrogen production from waste-derived synthesis gas. *Appl. Catal. B Environ.* **2019**, *249*, 72–81. [CrossRef]
6. Fan, M.-S.; Abdullah, A.Z.; Bhatia, S. Catalytic Technology for Carbon Dioxide Reforming of Methane to Synthesis Gas. *ChemCatChem.* **2009**, *1*, 192–208. [CrossRef]
7. Koo, K.Y.; Lee, S.-H.; Jung, U.H.; Roh, H.-S.; Yoon, W.L. Syngas production via combined steam and carbon dioxide reforming of methane over Ni–Ce/$MgAl_2O_4$ catalysts with enhanced coke resistance. *Fuel Process. Technol.* **2014**, *119*, 151–157. [CrossRef]

8. Jha, A.; Jeong, D.-W.; Lee, Y.-L.; Jang, W.-J.; Shim, J.-O.; Jeon, K.-W.; Rode, C.V.; Roh, H.-S. Chromium free high temperature water–gas shift catalyst for the production of hydrogen from waste derived synthesis gas. *Appl. Catal. A Gen.* **2016**, *522*, 21–31. [CrossRef]
9. Jang, W.-J.; Shim, J.-O.; Kim, H.-M.; Yoo, S.-Y.; Roh, H.-S. A review on dry reforming of methane in aspect of catalytic properties. *Catal. Today.* **2019**, *324*, 15–26. [CrossRef]
10. Jeon, K.-W.; Na, H.-S.; Lee, Y.-L.; Ahn, S.-Y.; Kim, K.-J.; Shim, J.-O.; Jang, W.-J.; Jeong, D.-W.; Nah, I.W.; Roh, H.-S. Catalytic deoxygenation of oleic acid over a Ni-$CeZrO_2$ catalyst. *Fuel* **2019**, *258*, 116179–116186. [CrossRef]
11. Ventura-Espinosa, D.; Sabater, S.; Carretero-Cerdán, A.; Baya, M.; Mata, J.A. High Production of Hydrogen on Demand from Silanes Catalyzed by Iridium Complexes as a Versatile Hydrogen Storage System. *ACS Catal.* **2018**, *8*, 2558–2566. [CrossRef]
12. Ismagilov, Z.R.; Matus, E.V.; Ismagilov, I.Z.; Sukhova, O.B.; Yashnik, S.A.; Ushakov, V.A.; Kerzhentsev, M.A. Hydrogen production through hydrocarbon fuel reforming processes over Ni based catalysts. *Catal. Today.* **2019**, *323*, 166–182. [CrossRef]
13. Kurtz, J.; Sprik, S.; Bradley, T.H. Review of transportation hydrogen infrastructure performance and reliability. *Int. J. Hydrogen Energ.* **2019**, *44*, 12010–12023. [CrossRef]
14. Shim, J.-O.; Na, H.-S.; Jha, A.; Jang, W.-J.; Jeong, D.-W.; Nah, I.W.; Jeon, B.-H.; Roh, H.-S. Effect of preparation method on the oxygen vacancy concentration of CeO_2-promoted Cu/γ-Al_2O_3 catalysts for HTS reactions. *Chem. Eng. J.* **2016**, *306*, 908–915. [CrossRef]
15. Jha, A.; Jeong, D.-W.; Shim, J.-O.; Jang, W.-J.; Lee, Y.-L.; Rode, C.V.; Roh, H.-S. Hydrogen production by the water-gas shift reaction using CuNi/Fe_2O_3 catalyst. *Catal. Sci. Technol.* **2015**, *5*, 2752–2760. [CrossRef]
16. Shim, J.-O.; Na, H.-S.; Ahn, S.-Y.; Jeon, K.-W.; Jang, W.-J.; Jeon, B.-H.; Roh, H.-S. An important parameter for synthesis of Al_2O_3 supported Cu-Zn catalysts in low-temperature water-gas shift reaction under practical reaction condition. *Int. J. Hydrogen Energ.* **2019**, *44*, 14853–14860. [CrossRef]
17. Lee, Y.-L.; Jha, A.; Jang, W.-J.; Shim, J.-O.; Rode, C.V.; Jeon, B.-H.; Bae, J.W.; Roh, H.-S. Effect of alkali and alkaline earth metal on Co/CeO_2 catalyst for the water-gas shift reaction of waste derived synthesis gas. *Appl. Catal. A Gen.* **2018**, *551*, 63–70. [CrossRef]
18. Jha, A.; Jeong, D.-W.; Jang, W.-J.; Lee, Y.-L.; Roh, H.-S. Hydrogen production from water–gas shift reaction over Ni–Cu–CeO_2 oxide catalyst: The effect of preparation methods. *Int. J. Hydrogen Energ.* **2015**, *40*, 9209–9216. [CrossRef]
19. Jeong, D.-W.; Jang, W.-J.; Shim, J.-O.; Han, W.-B.; Jeon, K.-W.; Seo, Y.-C.; Roh, H.-S.; Gu, J.H.; Lim, Y.T. A comparison study on high-temperature water–gas shift reaction over Fe/Al/Cu and Fe/Al/Ni catalysts using simulated waste-derived synthesis gas. *J. Mater. Cycles Waste.* **2014**, *16*, 650–656. [CrossRef]
20. Jeong, D.-W.; Jang, W.-J.; Jha, A.; Han, W.-B.; Jeon, K.-W.; Kim, S.-H.; Roh, H.-S. The Effect of Metal on Catalytic Performance over MFe_2O_4 Catalysts for High Temperature Water-Gas Shift Reaction. *J. Nanoelectron. Optoe.* **2015**, *10*, 530–534. [CrossRef]
21. Lee, D.-W.; Lee, M.S.; Lee, J.Y.; Kim, S.; Eom, H.-J.; Moon, D.J.; Lee, K.-Y. The review of Cr-free Fe-based catalysts for high-temperature water-gas shift reactions. *Catal. Today.* **2013**, *210*, 2–9. [CrossRef]
22. Jha, A.; Jeong, D.-W.; Lee, Y.-L.; Nah, I.W.; Roh, H.-S. Enhancing the catalytic performance of cobalt oxide by doping on ceria in the high temperature water–gas shift reaction. *RSC Adv.* **2015**, *5*, 103023–103029. [CrossRef]
23. Jha, A.; Lee, Y.-L.; Jang, W.-J.; Shim, J.-O.; Jeon, K.-W.; Na, H.-S.; Kim, H.-M.; Roh, H.-S.; Jeong, D.-W.; Jeon, S.G.; et al. Effect of the redox properties of support oxide over cobalt-based catalysts in high temperature water-gas shift reaction. *Mol. Catal.* **2017**, *433*, 145–152. [CrossRef]
24. Lee, Y.-L.; Jha, A.; Jang, W.-J.; Shim, J.-O.; Jeon, K.-W.; Na, H.-S.; Kim, H.-M.; Lee, D.-W.; Yoo, S.-Y.; Jeon, B.-H.; et al. Optimization of Cobalt Loading in Co-CeO_2 Catalyst for the High Temperature Water–Gas Shift Reaction. *Top. Catal.* **2017**, *60*, 721–726. [CrossRef]
25. Lee, Y.-L.; Kim, K.-J.; Jang, W.-J.; Shim, J.-O.; Jeon, K.-W.; Na, H.-S.; Kim, H.-M.; Bae, J.W.; Nam, S.C.; Jeon, B.-H.; et al. Increase in stability of BaCo/CeO_2 catalyst by optimizing the loading amount of Ba promoter for high-temperature water-gas shift reaction using waste-derived synthesis gas. *Renew. Energ.* **2020**, *145*, 2715–2722. [CrossRef]
26. Fazio, B.; Spadaro, L.; Trunfio, G.; Negro, J.; Arena, F. Raman scattering of MnO_x–CeO_x composite catalysts: Structural aspects and laser-heating effects. *J. Raman Spectrosc.* **2011**, *42*, 1583–1588. [CrossRef]

27. Arena, F.; Trunfio, G.; Negro, J.; Spadaro, L. Synthesis of highly dispersed $MnCeO_x$ catalysts via a novel "redox-precipitation" route. *Mater. Res. Bull.* **2008**, *43*, 539–545. [CrossRef]
28. Arena, F.; Chio, R.D.; Filiciottoa, L.; Trunfio, G.; Espro, C.; Palella, A.; Patti, A.; Spadaro, L. Probing the functionality of nanostructured $MnCeO_x$ catalysts in the carbon monoxide oxidation Part II. Reaction mechanism and kinetic modelling. *Appl. Catal. B Environ.* **2017**, *218*, 803–809. [CrossRef]
29. Arena, F.; Chio, R.D.; Espro, C.; Palella, A.; Spadaro, L. A definitive assessment of the CO oxidation pattern of a nanocomposite $MnCeO_x$ catalyst. *React. Chem. Eng.* **2018**, *3*, 293–300. [CrossRef]
30. Arena, F.; Chio, R.D.; Espro, C.; Fazio, B.; Palella, A.; Spadaro, L. A New Class of $MnCeO_x$ Materials for the Catalytic Gas Exhausts Emission Control: A Study of the CO Model Compound Oxidation. *Top. Catal.* **2019**, *62*, 259–265. [CrossRef]
31. Arena, F.; Famulari, P.; Interdonato, N.; Bonura, G.; Frusteri, F.; Spadaro, L. Physico-chemical properties and reactivity of Au/CeO_2 catalysts in total and selective oxidation of CO. *Catal. Today.* **2006**, *116*, 384–390. [CrossRef]
32. Liotta, L.F.; Ousmane, M.; Carlo, G.D.; Pantaleo, G.; Deganello, G.; Marcì, G.; Retailleau, L.; Giroir-Fendler, A. Total oxidation of propene at low temperature over Co_3O_4–CeO_2 mixed oxides: Role of surface oxygen vacancies and bulk oxygen mobility in the catalytic activity. *Appl. Catal. A Gen.* **2008**, *347*, 81–88. [CrossRef]
33. Reina, T.R.; Ivanova, S.; Delgado, J.J.; Ivanov, I.; Idakiev, V.; Tabakova, T.; Centeno, M.A.; Odriozola, J.A. Viability of Au/CeO_2–ZnO/Al_2O_3 Catalysts for Pure Hydrogen Production by the Water–Gas Shift Reaction. *ChemCatChem.* **2014**, *6*, 1401–1409. [CrossRef]
34. Reina, T.R.; Moreno, A.A.; Ivanova, S.; Odriozola, J.A.; Centeno, M.A. Influence of Vanadium or Cobalt Oxides on the CO Oxidation Behavior of $Au/MO_x/CeO_2$–Al_2O_3 Systems. *ChemCatChem.* **2012**, *4*, 512–520. [CrossRef]
35. Wang, J.A.; Morales, A.; Bokhimi, X.; Novaro, O.; López, T.; Gómez, R. Cationic and Anionic Vacancies in the Crystalline Phases of Sol−Gel Magnesia−Alumina Catalysts. *Chem. Mater.* **1999**, *11*, 308–313. [CrossRef]
36. Kakihana, M. Invited review "sol-gel" preparation of high temperature superconducting oxides. *J. Sol-Gel Sci. Techn.* **1996**, *6*, 7–55. [CrossRef]
37. Shojaie-Bahaabad, M.; Taheri-Nassaj, E. Economical synthesis of nano alumina powder using an aqueous sol–gel method. *Mater. Lett.* **2008**, *62*, 3364–3366. [CrossRef]
38. Avgouropoulos, G.; Ioannides, T.; Matralis, H. Influence of the preparation method on the performance of CuO–CeO_2 catalysts for the selective oxidation of CO. *Appl. Catal. B Environ.* **2005**, *56*, 87–93. [CrossRef]
39. Qiao, D.; Lu, G.; Liu, X.; Guo, Y.; Wang, Y.; Guo, Y. Preparation of $Ce_{1-x}Fe_xO_2$ solid solution and its catalytic performance for oxidation of CH_4 and CO. *J. Mater. Sci.* **2011**, *46*, 3500–3506. [CrossRef]
40. Megarajan, S.K.; Rayalu, S.; Teraoka, Y.; Labhsetwar, N. High NO oxidation catalytic activity on non-noble metal based cobalt-ceria catalyst for diesel soot oxidation. *J. Mol. Catal. A Chem.* **2014**, *385*, 112–118. [CrossRef]
41. Na, H.-S.; Ahn, S.-Y.; Shim, J.-O.; Jeon, K.-W.; Kim, H.-M.; Lee, Y.-L.; Jang, W.-J.; Jeon, B.-H.; Roh, H.-S. Effect of precipitation on physico-chemical and catalytic properties of Cu-Zn-Al catalyst for water-gas shift reaction. *Korean, J. Chem. Eng.* **2019**, *36*, 1243–1248. [CrossRef]
42. Shim, J.-O.; Jeon, K.-W.; Jang, W.-J.; Na, H.-S.; Cho, J.-W.; Kim, H.-M.; Lee, Y.-L.; Jeong, D.-W.; Roh, H.-S.; Ko, C.H. Facile production of biofuel via solvent-free deoxygenation of oleic acid using a CoMo catalyst. *Appl. Catal. B Environ.* **2018**, *239*, 644–653. [CrossRef]
43. Shim, J.-O.; Jang, W.-J.; Jeon, K.-W.; Lee, D.-W.; Na, H.-S.; Kim, H.-M.; Lee, Y.-L.; Yoo, S.-Y.; Jeon, B.-H.; Roh, H.-S.; et al. Petroleum like biodiesel production by catalytic decarboxylation of oleic acid over $Pd/Ce\text{-}ZrO_2$ under solvent-free condition. *Appl. Catal. A Gen.* **2018**, *563*, 163–169. [CrossRef]
44. Banerjee, A.M.; Pai, M.R.; Tewari, R.; Raje, N.; Tripathi, A.K.; Bharadwaj, S.R.; Das, D. A comprehensive study on Pt/Al_2O_3 granular catalyst used for sulfuric acid decomposition step in sulfur–iodine thermochemical cycle: Changes in catalyst structure, morphology and metal-support interaction. *Appl. Catal. B Environ.* **2015**, *162*, 327–337. [CrossRef]
45. Zhang, S.; Li, Y.; Huang, J.; Lee, J.; Kim, D.H.; Frenkel, A.I.; Kim, T. Effects of Molecular and Electronic Structures in CoO_x/CeO_2 Catalysts on NO Reduction by CO. *J. Phys. Chem. C.* **2019**, *123*, 7166–7177. [CrossRef]
46. Gómez, L.E.; Boix, A.V.; Miró, E.E. Co/ZrO_2, Co/CeO_2 and MnCoCe structured catalysts for COPrOx. *Catal. Today.* **2013**, *216*, 246–253. [CrossRef]

47. Gómez, L.E.; Múnera, J.F.; Sollier, B.M.; Miró, E.E.; Boix, A.V. Raman in situ characterization of the species present in Co/CeO_2 and Co/ZrO_2 catalysts during the COPrOx reaction. *Int. J. Hydrogen Energ.* **2016**, *41*, 4993–5002. [CrossRef]
48. Martínez-Arias, A.; Gamarra, D.; Fernández-García, M.; Wang, X.Q.; Hanson, J.C.; Rodriguez, J.A. Comparative study on redox properties of nanosized CeO_2 and CuO/CeO_2 under CO/O_2. *J. Catal.* **2006**, *240*, 1–7. [CrossRef]
49. Jang, W.-J.; Kim, H.-M.; Shim, J.-O.; Yoo, S.-Y.; Jeon, K.-W.; Na, H.-S.; Lee, Y.-L.; Jeong, D.-W.; Bae, J.W.; Nah, I.W.; et al. Key properties of Ni-MgO-CeO_2, Ni-MgO-ZrO_2, and Ni-MgO-$Ce_{(1-x)}Zr_{(x)}O_2$ catalysts for the reforming of methane with carbon dioxide. *Green Chem.* **2018**, *20*, 1621–1633. [CrossRef]
50. Biesinger, M.C.; Payne, B.P.; Grosvenor, A.P.; Lau, L.W.M.; Gerson, A.R.; Smart, R.S.C. Resolving surface chemical states in XPS analysis of first row transition metals, oxides and hydroxides: Cr, Mn, Fe, Co and Ni. *Appl. Surf. Sci.* **2011**, *257*, 2717–2730. [CrossRef]
51. Idriss, H.; Diagne, C.; Hindermann, J.P.; Kiennemann, A.; Barteau, M.A. Reactions of Acetaldehyde on CeO_2 and CeO_2-Supported Catalysts. *J. Catal.* **1995**, *155*, 219–237. [CrossRef]
52. Kumar, P.A.; Tanwar, M.D.; Russo, N.; Pirone, R.; Fino, D. Synthesis and catalytic properties of CeO_2 and Co/CeO_2 nanofibres for diesel soot combustion. *Catal. Today.* **2012**, *184*, 279–287. [CrossRef]
53. Lin, S.S.-Y.; Kim, D.H.; Engelhard, M.H.; Ha, S.Y. Water-induced formation of cobalt oxides over supported cobalt/ceria–zirconia catalysts under ethanol-steam conditions. *J. Catal.* **2010**, *273*, 229–235. [CrossRef]
54. Aramendía, M.A.; Colmenares, J.C.; Marinas, A.; Marinas, J.M.; Moreno, J.M.; Navío, J.A.; Urbano, F.J. Effect of the redox treatment of Pt/TiO_2 system on its photocatalytic behaviour in the gas phase selective photooxidation of propan-2-ol. *Catal. Today.* **2007**, *128*, 235–244. [CrossRef]
55. Weerachawanasak, P.; Mekasuwandumrong, O.; Arai, M.; Fujita, S.-I.; Praserthdam, P.; Panpranot, J. Effect of strong metal–support interaction on the catalytic performance of Pd/TiO_2 in the liquid-phase semihydrogenation of phenylacetylene. *J. Catal.* **2009**, *262*, 199–205. [CrossRef]
56. Kim, W.-J.; Moon, S.H. Modified Pd catalysts for the selective hydrogenation of acetylene. *Catal. Today.* **2012**, *185*, 2–16. [CrossRef]
57. Fichtl, M.B.; Schumann, J.; Kasatkin, I.; Jacobsen, N.; Behrens, M.; Schlögl, R.; Muhler, M.; Hinrichsen, O. Counting of Oxygen Defects versus Metal Surface Sites in Methanol Synthesis Catalysts by Different Probe Molecules. *Angew. Chem. Int. Ed.* **2014**, *53*, 7043–7047. [CrossRef]
58. Wang, N.; Qian, W.; Chu, W.; Wei, F. Crystal-plane effect of nanoscale CeO_2 on the catalytic performance of Ni/CeO_2 catalysts for methane dry reforming. *Catal. Sci. Technol.* **2016**, *6*, 3594–3605. [CrossRef]
59. Feng, X.; Guo, J.; Wen, X.; Xu, M.; Chu, Y.; Yuan, S. Enhancing performance of Co/CeO_2 catalyst by Sr doping for catalytic combustion of toluene. *Appl. Surf. Sci.* **2018**, *445*, 145–153. [CrossRef]
60. Zhan, Y.; Liu, Y.; Peng, X.; Zhao, W.; Zhang, Y.; Wang, X.; Au, C.; Jiang, L. Molecular-level understanding of reaction path optimization as a function of shape concerning the metal–support interaction effect of Co/CeO_2 on water-gas shift catalysis. *Catal. Sci. Technol.* **2019**, *9*, 4928–4937. [CrossRef]
61. Gamboa-Rosales, N.K.; Ayastuy, J.L.; Iglesias-González, A.; González-Marcos, M.P.; Gutiérrez-Ortiz, M.A. Oxygen-enhanced WGS over ceria-supported Au–Co_3O_4 bimetallic catalysts. *Chem. Eng. J.* **2012**, *207–208*, 49–56. [CrossRef]
62. Tepamatr, P.; Laosiripojana, N.; Sesuk, T.; Charojrochkul, S. Effect of samarium and praseodymium addition on water gas shift performance of Co/CeO_2 catalysts. *J. Rare. Earth.* **2019**, in press. [CrossRef]
63. Jianqiang, W.; Meiqing, S.; Jun, W.; Jidong, G.; Jie, M.; Shuangxi, L. Effect of cobalt doping on ceria-zirconia mixed oxide: Structural characteristics, oxygen storage/release capacity and three-way catalytic performance. *J. Rare. Earth.* **2012**, *30*, 878–883. [CrossRef]
64. Li, C.; Li, Z.; Park, S.B.; Hong, G.H.; Park, J.S.; Oh, H.Y.; Kim, J.M. Ordered Mesoporous Cu–Co–CeO_2 Catalyst for Water-Gas Shift Reaction at High Temperature. *J. Nanosci. Nanotechno.* **2017**, *17*, 8149–8152. [CrossRef]